THE JOURNAL OF PHYSICAL CHEMISTRY A

Article

Cite This: J. Phys. Chem. A 2018, 122, 9886−9893

pubs.acs.org/JPCA

Photoelectron Spectroscopy and Theoretical Study of $Cr_nSi_{15-n}^-$ (n = 1−3): Effects of Doping Cr Atoms on the Structural and Magnetic Properties

Bin Yang, Hongguang Xu, Xiling Xu,* and Weijun Zheng*

Beijing National Laboratory for Molecular Sciences, State Key Laboratory of Molecular Reaction Dynamics, Institute of Chemistry, Chinese Academy of Sciences, Beijing 100190, China

University of Chinese Academy of Sciences, Beijing 100049, China

Supporting Information

ABSTRACT: $Cr_nSi_{15-n}^-$ (n = 1−3) clusters were investigated by using size-selected anion photoelectron spectroscopy combined with density functional theory calculations. The results show that the most stable structure of $CrSi_{14}^-$ is of C_{2v} symmetry with the Cr atom encapsulated in a Si_{14} cage which can be viewed as a boat-shaped Si_{10} unit capped by four additional silicon atoms. A large HOMO−LUMO gap of neutral $CrSi_{14}$ is confirmed based on the photoelectron spectrum of $CrSi_{14}^-$ anion. $Cr_2Si_{13}^-$ has two isomers nearly degenerate in energy: one can be characterized as one Si atom interacting with a Cr_2Si_{12} hexagonal prism while the other can be viewed as one Si atom capping a distorted Cr_2Si_{12} hexagonal antiprism. $Cr_3Si_{12}^-$ has a D_{6d} symmetric wheel structure in which three Cr atoms form an axle surrounded by 12 Si atoms. The magnetic moments of $CrSi_{14}^-$, $Cr_2Si_{13}^-$, and $Cr_3Si_{12}^-$ increase from 1 to 3 μB and then to 7 μB with the increasing number of Cr atoms in the clusters. The magnetic moments of $Cr_2Si_{13}^-$ and $Cr_3Si_{12}^-$ are mainly contributed by the surface Cr atoms.

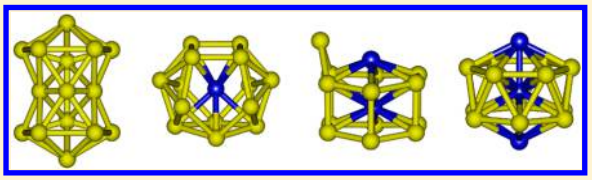

1. INTRODUCTION

Transition-metal-doped silicon clusters have been investigated extensively by experiments[1−10] and theoretical calculations[11−18] in the past decades because transition metals can stabilize the special geometrical structure of silicon clusters and introduce novel chemical or physical properties to the silicon clusters. Chromium−silicon alloys have important applications in nanomaterials and electronics.[19] Many research groups had studied chromium−silicon clusters with experimental[20−23] and theoretical methods.[24−35] Beck investigated MSi_n^+ (M = Cr, Mo, W) clusters with mass spectrometry.[20,21] Zheng and co-workers investigated $CrSi_n^-$ clusters using mass-selected anion photoelectron spectroscopy.[22,23] Lievens and co-workers conducted mass spectrometric stability study on a series of binary clusters including $CrSi_{14}$.[24] Han and co-workers studied the structures of $CrSi_{1-6}$[25] and MSi_{15} (M = Cr, Mo, W)[26] using density functional theory (DFT) calculations. The structure evolution and growth behavior of $CrSi_n$ from n = 8 up to 17 were studied by Kawamura et al.[27] and Guo et al.[28] The structures and electron-counting rule for the stability of $CrSi_{12}$ were investigated by Khanna and co-workers with first-principle theoretical method.[29,30] Several theoretical works were also dedicated to investigate the cage structures of $CrSi_{14}$[31] and $CrSi_{15,16}$.[32,33] The structures and magnetic properties of M_2Si_{1-8} (M = Cr, Mn) were studied with DFT methods by Robles et al.[34] and those of M_2Si_{18} (M = Ti−Zn) by Ji and Luo.[35]

In this work, we examine the changes in structural and magnetic properties when the Si atoms of silicon clusters were gradually replaced by the Cr atoms. This work is focused on the structures and magnetic properties of chromium-doped silicon clusters composed of 15 atoms ($Cr_nSi_{15-n}^-$) using mass-selected anion photoelectron spectroscopy combined with DFT calculations. Our results show that the geometric structures become more symmetric when the number of Cr atoms increases from 1 to 3. Also, the magnetic moments of $Cr_nSi_{15-n}^-$ increase with the increasing number of Cr atoms. It is found that $Cr_3Si_{12}^-$ has a D_{6d} symmetric wheel structure with aromaticity.

2. EXPERIMENTAL AND THEORETICAL METHODS

2.1. Experimental Method. The experiments were conducted on a home-built apparatus consisting of a laser vaporization cluster source, a time-of-flight mass spectrometer, and a magnetic-bottle photoelectron spectrometer, which has been described elsewhere.[36] The Cr−Si cluster anions were generated in the laser vaporization source by laser ablation of a rotating and translating disk target of the mixture of chromium and isotopically enriched silicon (13 mm diameter, Cr:^{28}Si mole ratio 3:2, ^{28}Si 99.989%) with the second harmonic light pulses (532 nm) of a nanosecond Nd:YAG laser (Continuum

Received: October 30, 2018
Revised: November 25, 2018
Published: December 3, 2018

DOI: 10.1021/acs.jpca.8b10588
J. Phys. Chem. A 2018, 122, 9886−9893

Surelite II-10). The typical laser power used in this work is about 10 mJ/pulse. Helium gas with about 3 atm backing pressure was allowed to expand through a pulsed valve (General Valve Series 9) into the source to cool the formed clusters. The generated cluster anions were mass-analyzed with the time-of-flight mass spectrometer. $CrSi_{14}^-$, $Cr_2Si_{13}^-$, and $Cr_3Si_{12}^-$ were each selected with a mass gate, decelerated by a momentum decelerator, and crossed with the beam of another Nd:YAG laser (Continuum Surelite II-10, 266 nm) in the photodetachment region. The electrons from photodetachment were energy-analyzed by the magnetic-bottle photoelectron spectrometer. The resolution of the magnetic-bottle photoelectron spectrometer was about 40 meV at electron kinetic energy of 1 eV. The photoelectron spectra were calibrated with the spectra of Cu^- and Au^- taken at similar conditions.

2.2. Theoretical Method. An unbiased search for structures of $Cr_nSi_{15-n}^-$ (n = 1−3) were carried out using the crystal structure analysis by particle swarm optimization (CALYPSO) software based on particle swarm algorithm.[37,38] Many structures reported in the literature also were taken into account as initial structures. The low-lying structures obtained were further optimized using the Gaussian 09 program package.[39] Geometry optimizations and frequency analysis were carried out with the Perdew−Burke−Enzerhof (PBE) functional based on the generalized gradient approximation (GGA).[40] Pople's all electron 6-311+G(d) basis set was used both for Cr atoms[41] and Si atoms.[42] All geometry optimizations were performed without any symmetry constraint. Various spin-multiplicities were considered to obtain the lowest energy spin state as a Cr atom has six unpaired electrons ($3d^54s^1$). Harmonic vibrational frequencies were calculated to confirm that the structures correspond to the true local minima. The zero-point vibrational energy corrections were included for the relative energies of isomers. Spin magnetic moments, atomic charges, and electronic configurations were evaluated based on natural bond analysis with the natural bond orbital (NBO) version 3.1 program[43−50] implemented in the Gaussian 09 package,[39] which are carried out at the PBE/6-31+G(d) level since NBO is independent of basis set. In addition, the aromaticity is analyzed by anisotropy of the induced current density.[51,52] The partial and total density of states are conducted by Multiwfn wave function analysis program.[53] To understand the influence of difference functionals, the low-lying structures of the $Cr_nSi_{15-n}^-$ (n = 1−3) clusters were calculated by Becke's three-parameter and Lee−Yang−Parr's gradient-corrected correlation hybrid functional (B3LYP)[54,55] with 6-311+G(d) basis set. The calculated results of B3LYP functional are in agreement with those of PBE functional in general except that the simulated spectra using B3LYP functional are in slightly worse agreement with the experimental spectra. Previous theoretical studies showed that the PBE functional is suitable for calculating the structures and properties of Cr-doped Si clusters.[17,29] Thus, we mainly present the results from PBE functional here.

3. EXPERIMENTAL AND THEORETICAL RESULTS

The photoelectron spectra of $Cr_nSi_{15-n}^-$ (n = 1−3) clusters recorded at 266 nm wavelength are shown in Figure 1. The experimental vertical detachment energies (VDEs) and adiabatic detachment energies (ADEs) of $Cr_nSi_{15-n}^-$ (n = 1−3) clusters obtained from their photoelectron spectra are summarized in Table 1. The VDEs of $Cr_nSi_{15-n}^-$ (n = 1−3) clusters were evaluated from the maxima of the first peaks in the spectra, and the ADEs were determined by drawing a straight line along the leading edge of the first peaks to cross the baseline of spectra and adding the instrument resolution to the electron binding energy (EBE) values at the crossing points.

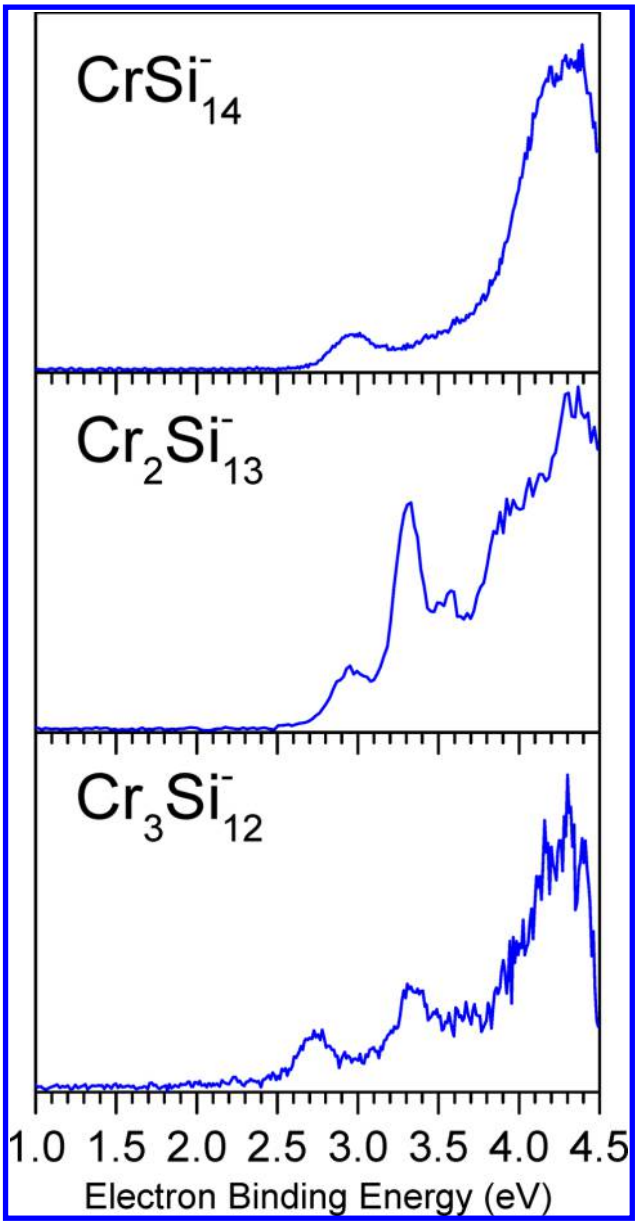

Figure 1. Photoelectron spectra of $Cr_nSi_{15-n}^-$ (n = 1−3) clusters recorded with 266 nm photons.

The spectrum of $CrSi_{14}^-$ possesses a small peak centered at 2.97 eV followed by an unresolved high-intensity broad feature between 4.20 and 4.39 eV. In the spectrum of $Cr_2Si_{13}^-$, there are four peaks centered at 2.95, 3.31, 3.49, and 3.58 eV, respectively, and some unresolved broad peaks above 3.92 eV. As for the spectrum of $Cr_3Si_{12}^-$, there are two peaks centered at 2.73 and 3.34 eV, a low-intensity peak centered at 3.67 eV, and four barely resolved peaks at 3.99, 4.16, 4.30, and 4.41 eV, respectively.

The typical low-lying isomers of $Cr_nSi_{15-n}^-$ (n = 1−3) clusters obtained from DFT calculations are presented in Figure 2 with the most stable ones on the left. Their relative

DOI: 10.1021/acs.jpca.8b10588
J. Phys. Chem. A 2018, 122, 9886−9893

Table 1. Relative Energies, VDEs, and ADEs of $Cr_nSi_{15-n}^-$ (n = 1−3) Isomers Are Calculated at the PBE/6-311+G(d) Level[a]

isomer		state	sym.	ΔE[b] (eV)	VDE (eV) theor.[b]	VDE (eV) expt.[c]	ADE (eV) theor.[b]	ADE (eV) expt.[c]
$CrSi_{14}^-$	**1A**	$^2A_1$	C_{2v}	0.00	2.89	2.97	2.82	2.74
	1B	$^2A_1$	C_{2v}	0.21	2.87		2.81	
	1C	$^2A''$	C_s	0.26	3.57		3.17	
	1D	$^2A_{1g}$	D_{3d}	0.35	3.34		3.24	
$Cr_2Si_{13}^-$	**2A**	$^4A'$	C_s	0.00	3.01	2.95	2.92	2.76
	2B	$^4A''$	C_s	0.01	2.89		2.71	
	2C	$^6A'$	C_s	0.25	3.05		2.96	
	2D	$^4A''$	C_s	0.93	3.07		2.92	
$Cr_3Si_{12}^-$	**3A**	$^8B_1$	D_{6d}	0.00	2.56	2.73	2.71	2.52
	3B	^6A	C_3	0.71	2.75		1.81	
	3C	^6A	C_1	0.79	3.02		2.97	
	3D	^8A	C_1	0.82	2.86		2.80	

[a]The isomers labeled in bold are the most probable isomers in the experiments. [b]These energies are calculated at the PBE/6-311+G(d) level. [c]The uncertainties of experimental VDEs and ADEs are ±0.08 eV.

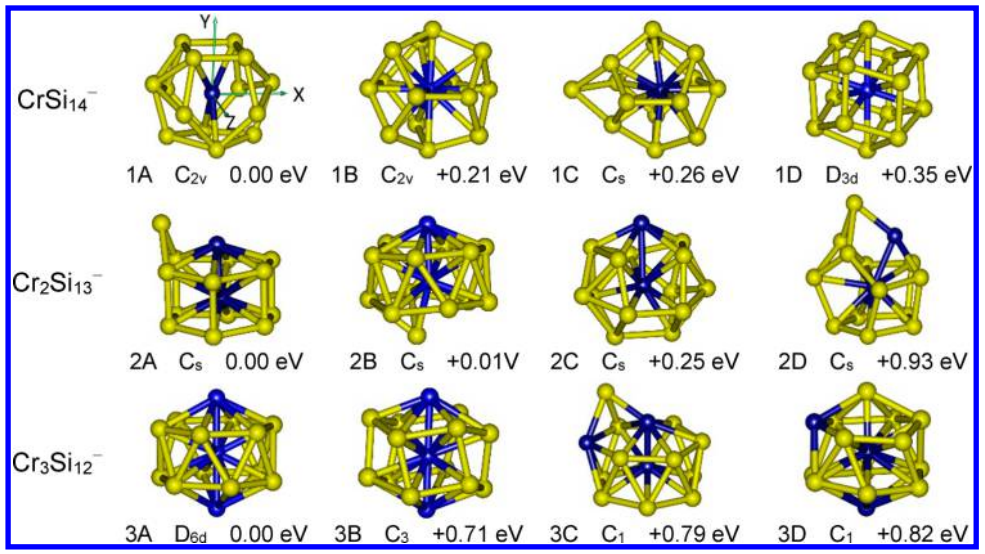

Figure 2. Low-lying isomers of $Cr_nSi_{15-n}^-$ (n = 1−3) clusters. The relative energies to the most stable isomers are listed under the geometric structures. Yellow and blue balls stand for the Si and Cr atoms, respectively.

energies and theoretical VDEs and ADEs are summarized and compared to the experimental values in Table 1. We simulated the photoelectron spectra of the low-lying isomers on the basis of theoretically generalized Koopmans' theorem (GKT)[56,57] and compared the simulated spectra to the experimental spectra in Figure 3. Additionally, we also optimized the structures of neutral Cr_nSi_{15-n} (n = 1−3) clusters at the PBE/6-311+G(d) level and displayed them in Figure 4.

3.1. $CrSi_{14}^-$ and $CrSi_{14}$. The most stable isomer (1A) of $CrSi_{14}^-$ has C_{2v} symmetry with the Cr atom encapsulated in a Si_{14} cage which can be viewed as a boat-shaped Si_{10} unit capped by four additional silicon atoms. The calculated VDE of isomer 1A (2.89 eV) is in good agreement with the experimental value (2.97 eV), and its simulated spectrum matches the peak positions, patterns, and intensities of the experimental spectrum very well. Isomer 1B is a polyhedral cage made of three quadrangles and six pentagons. The theoretical VDE (2.87 eV) of isomer 1B is also close to the experimental value, but isomer 1B is higher in energy than 1A by 0.21 eV. Isomer 1C is converted from isomer 1B with one of the Si atoms protruding and the silicon cage shrinking slightly. Isomer 1D is a polyhedron consisting of 12 rectangles, which can also be viewed as a distorted capped hexagonal prism composed of two chair-shaped Si_6 rings and two capping Si atoms. Isomers 1C and 1D are higher than 1A in energy by 0.26 and 0.35 eV, respectively, and their calculated VDEs are much higher than the experimental value. Thereby, isomer 1A is the most probable one detected in our experiments.

The most stable structure of neutral $CrSi_{14}$ (1A′) is also a C_{2v} symmetric structure with the Cr atom encapsulated in a Si_{14} cage, analogous to that of its anionic counterpart (1A, $CrSi_{14}^-$). The other low-lying isomers of $CrSi_{14}$ are higher in energy than the most stable one (1A′) by at least 0.20 eV. The structures of $CrSi_{14}$ and $CrSi_{14}^-$ found in this work are consistent with previous theoretical studies.[27−31] Khanna and co-workers suggested that $CrSi_{14}$ follows the 18-electron rule and exhibits the characterristics of magic cluster.[29] In this work, the experimental spectrum and simulated spectrum of $CrSi_{14}^-$ show a large gap between the first peak and second peak, indicating that the neutral $CrSi_{14}$ has a large HOMO−LUMO gap. Therefore, our experimental spectrum and

DOI: 10.1021/acs.jpca.8b10588
J. Phys. Chem. A 2018, 122, 9886−9893

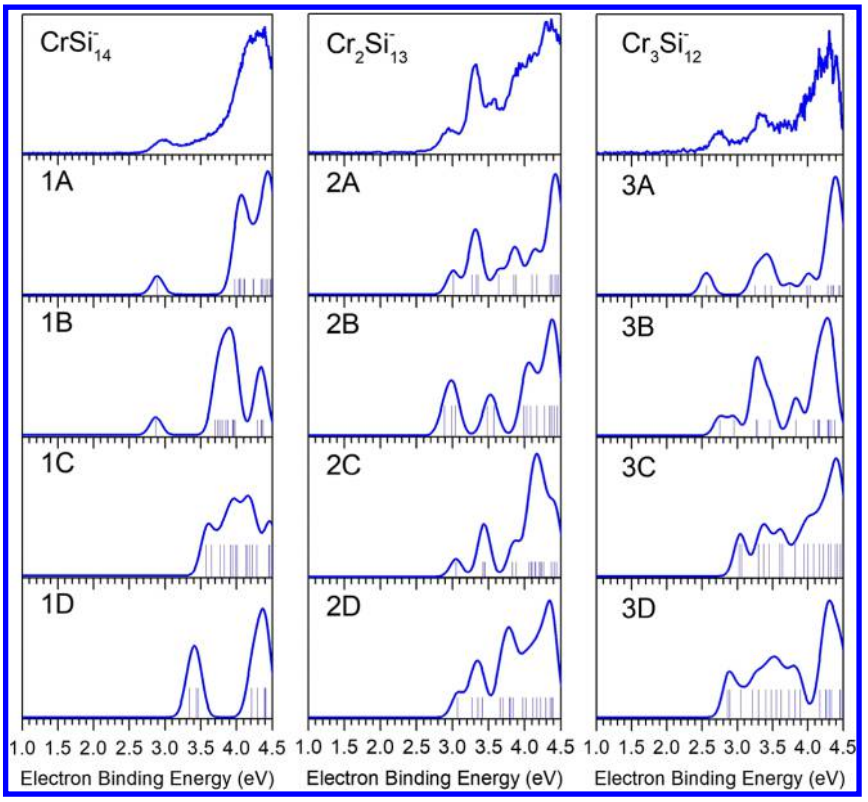

Figure 3. Comparison between the experimental photoelectron spectra and the simulated spectra of the low-lying isomers of $Cr_nSi_{15-n}^-$ (n = 1−3). The simulated spectra were obtained by fitting the distribution of the transition lines with unit area Gaussian functions of 0.20 eV full-width at half-maximum.

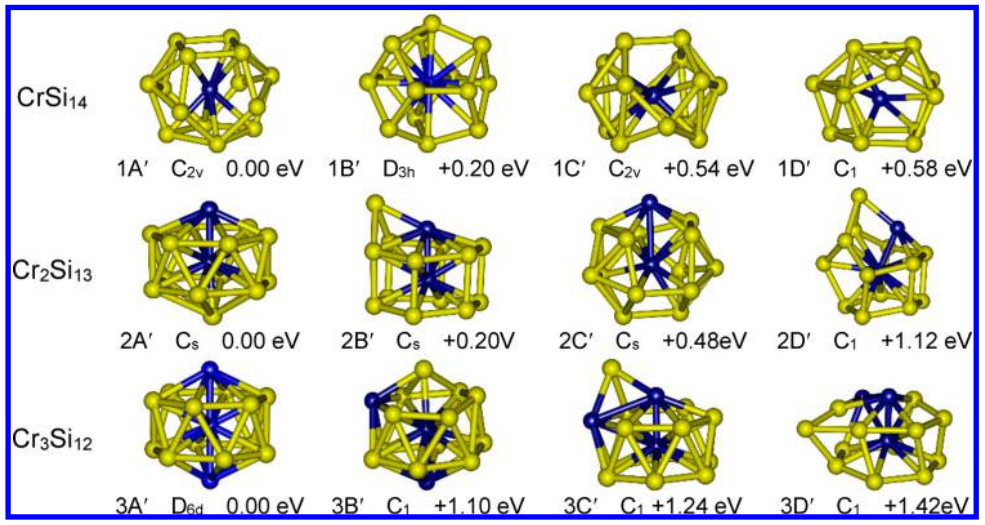

Figure 4. Low-lying isomers of Cr_nSi_{15-n} (n = 1−3) clusters. The relative energies to the most stable isomers are listed under the geometric structures. Yellow and blue balls stand for the Si and Cr atoms, respectively.

theoretical calculations confirm the prediction of Khanna and co-workers.

The previous studies on pure silicon clusters show that the lowest-energy structure of Si_{15}^- consists of a face-sharing fusion of two deformed TTP with C_{2v} symmetry.[58,59] It appears that the Si_{15}^- prolate structure transforms to near-spherical configuration when one of the Si atoms is replaced by a Cr atom ($CrSi_{14}^{-/0}$). It will be shown later that the structure evolves to a high symmetric one when three Si atoms of Si_{15}^- are replaced by three Cr atoms ($Cr_3Si_{12}^{-/0}$).

3.2. $Cr_2Si_{13}^-$ and Cr_2Si_{13}. The first two isomers of $Cr_2Si_{13}^-$ (2A and 2B) are nearly degenerate in energy, with isomer 2B higher than 2A by only 0.01 eV. Isomer 2A can be regarded as deriving from a hexagonal prism, with one Cr atom encapsulated inside a Si_{12} cage, the second Cr atom face-capping the top of the hexagonal prism, and the additional Si atom attaching to one side of the upper Si_6 ring. The Cr−Cr bond length in isomer 2A is about 2.30 Å. Isomer 2B is a distorted hexagonal antiprism, with the last Si atom capping the hexagonal antiprism from the opposite side of the external Cr atom. The theoretical VDEs (3.01 and 2.89 eV) of isomers

DOI: 10.1021/acs.jpca.8b10588
J. Phys. Chem. A 2018, 122, 9886−9893

2A and 2B are both in good agreement with the experimental value (2.95 eV). The simulated spectrum of isomer 2A can match most of the peak positions and patterns of the experimental spectrum and that of isomer 2B also matches the experimental peaks at 2.95, 3.49, 4.11, and 4.33 eV. The combination of the simulated spectra of isomers 2A and 2B can fit the experimental spectrum very well. Isomers 2C and 2D are less stable than 2A by 0.25 and 0.93 eV, respectively. Therefore, the contribution of isomers 2C and 2D to the experimental spectrum can be negligible, and isomers 2A and 2B are the major ones contributing to the experimental spectrum.

For neutral Cr_2Si_{13}, the most stable isomer (2A′) has a hexagonal antiprism structure, with the last Si atom capping the hexagonal antiprism from the opposite side of the external Cr atom. It resembles the second isomer (2B) of $Cr_2Si_{13}^-$ but in slightly more symmetric shape. The Cr−Cr bond length in isomer 2A′ is about 2.29 Å. The second isomer of Cr_2Si_{13} (2B′) is somewhat similar to the first isomer (2A) of $Cr_2Si_{13}^-$. The switch of the stability order indicates that the number of electrons has an effect on the geometric structures.

3.3. $Cr_3Si_{12}^-$ and Cr_3Si_{12}. As for $Cr_3Si_{12}^-$, the most stable structure (3A) is a D_{6d} symmetric antihexagonal prism in which a Cr−Cr−Cr central axle is surrounded by two Si_6 rings, which is similar to the D_{6d} wheel structure of $V_3Si_{12}^-$.[60,61] The calculated VDE of isomer 3A is 2.56 eV, in agreement with the experimental VDE (2.73 eV). The simulated spectrum of 3A is also in good agreement with the experimental spectrum of $Cr_3Si_{12}^-$. The other isomers (3B, 3C, and 3D) are much higher in energy than isomer 3A by 0.71, 0.79, and 0.82 eV, respectively. Therefore, isomer 3A is the most probable one detected in our experiments.

The most stable structure of neutral Cr_3Si_{12} (3A′) is also an antihexagonal prism with D_{6d} symmetry, similar to its anionic counterpart. Isomer 3A′ is lower in energy than the second isomer (3B′) by 1.10 eV, demonstrating that the D_{6d} symmetric structure is very stable. The Cr−Cr bond lengths in Cr_3Si_{12} are 2.27 Å, while those in $Cr_3Si_{12}^-$ are 2.33 Å. The Si−Si bond lengths of the Si_6 rings are calculated to be 2.43 Å for anion and neutral; the Si−Si bond lengths between two Si_6 rings are 2.53 Å for Cr_3Si_{12} and 2.54 Å for $Cr_3Si_{12}^-$. These indicate that the geometric structure of neutral Cr_3Si_{12} is slightly more compact than that of its anionic counterpart. It is worth mentioning that the Cr−Cr interactions in $Cr_3Si_{12}^{-/0}$ are quite strong because the Cr−Cr bond lengths in $Cr_3Si_{12}^{-/0}$ are longer than that in the Cr_2 molecule (1.68 Å)[62] but shorter than that in metallic chromium (2.51 Å).[63]

4. DISCUSSION

4.1. Charge Distributions and Magnetic Properties of $CrSi_{14}^-$, $Cr_2Si_{13}^-$, and $Cr_3Si_{12}^-$. We conducted natural population analysis (NPA) on the most stable structures of $CrSi_{14}^-$, $Cr_2Si_{13}^-$, and $Cr_3Si_{12}^-$. The charges, magnetic moments, and electron configurations of the Cr atoms in these species are presented in Table 2 (those of Si atoms are shown in the Supporting Information, Table S1). For $CrSi_{14}^-$, the interior Cr atom carries considerable negative charges (−2.91 e) while all the Si atoms have small amounts of positive charges (+0.12 to 0.16 e). Similarly, for $Cr_2Si_{13}^-$, the charges on the internal Cr atom are about −2.17 e while that on the surface Cr atom are about −0.40 e. As for $Cr_3Si_{12}^-$, the internal Cr atom carries −2.42 e charges whereas the two surface Cr atoms and 12 Si atoms have small amounts of positive charges.

Table 2. NPA Charges, Chromium Atomic Moments (μ_{Cr}), Total Magnetic Moments (μ_T), and Natural Electron Configuration of the Most Stable Isomers of $Cr_nSi_{15-n}^-$ (n = 1−3)

cluster	atom	NPA on Cr atom	μ_{Cr} [μB]	μ_T [μB]	natural electron configuration on Cr atom
$CrSi_{14}^-$	Cr_i	−2.91	0.72	1	$3d^{7.94}4s^{0.55}4p^{0.14}4d^{0.23}$
$Cr_2Si_{13}^-$	Cr_i	−2.17	−0.57	3	$3d^{7.30}4s^{0.54}4p^{0.08}4d^{0.22}$
	Cr_s	−0.40	2.86		$3d^{5.72}4s^{0.42}4p^{0.09}4d^{0.15}$
$Cr_3Si_{12}^-$	Cr_i	−2.42	−0.29	7	$3d^{7.52}4s^{0.56}4p^{0.03}4d^{0.23}$
	Cr_{s1}	0.04	3.66		$3d^{5.49}4s^{0.28}4p^{0.10}4d^{0.07}$
	Cr_{s2}	0.04	3.66		$3d^{5.49}4s^{0.28}4p^{0.10}4d^{0.07}$

It is found that the electron numbers on the Si 3s orbitals decrease by ∼0.5−0.6 while those on the Si 3p orbitals increase by ∼0.4−0.5 (Table S1), designating there are strong hybridizations between the Si 3s and 3p orbitals and there are electrons loss for the Si atoms. From the natural electron configurations on Cr (Table 2), it can be seen that the 3d orbitals of the internal Cr atoms gain a significant number of electrons, which is more likely due to the strong interaction between the Cr 3d orbitals and the Si 3s and 3p orbitals. The total magnetic moments of $CrSi_{14}^-$, $Cr_2Si_{13}^-$, and $Cr_3Si_{12}^-$ are calculated to be 1, 3, and 7 μB, respectively (Table 2). The local magnetic moments on the Si atoms are very small. The local magnetic moments on the interior Cr atoms are 0.72 μB for $CrSi_{14}^-$, −0.57 μB for $Cr_2Si_{13}^-$, and −0.29 μB for $Cr_3Si_{12}^-$, respectively. The surface Cr atom of $Cr_2Si_{13}^-$ has local magnetic moments of 2.86 μB, whereas the two surface Cr atoms of $Cr_3Si_{12}^-$ each have local magnetic moments of 3.66 μB. Overall, the magnetic moment of interior Cr atom is quenched because of the interaction with the Si atoms. The magnetic moments of $Cr_2Si_{13}^-$ and $Cr_3Si_{12}^-$ are mainly contributed by the surface Cr atoms. It is in agreement with the charge distributions because the d orbitals of the surface Cr atoms have more unpaired electrons.

4.2. Density of States and Electron Delocalization of $Cr_3Si_{12}^-$. We investigated the partial density of states (PDOS) of $Cr_3Si_{12}^-$ and presented the results in Figure 5. The Cr−Si and Cr−Cr interactions can be interpreted based on Figure 5. It can be seen that, for the surface Cr atoms, there are strong overlaps between Cr_s d and Si_6 p. For the interior Cr atom, very strong overlaps also exist at −1.05 to −2.75 eV between Cr_i d and Si_6 p. The overlaps between Cr d and Si p states confirm the NPA analysis that strong interaction exists between the Cr 3d orbitals and the Si 3p orbitals, which contribute to the stability of $Cr_3Si_{12}^-$. Regarding the Cr−Cr interaction, the majority spin of the interior and surface Cr atoms overlaps at the Fermi level and at the location between −1.39 and −2.37 eV, indicating the Cr−Cr interaction is also strong. In addition, it is found that the majority spin of Cr_s d has a large feature at −0.85 eV while the Cr_i d shows a large feature of minority spin at 1.86 eV, which is in agreement with the local magnetic moments of the Cr atoms (the surface Cr atoms carry the most magnetic moments, while the interior Cr has a small local magnetic moment).

To further understand the stability and electron delocalization of $Cr_3Si_{12}^-$, we conducted the anisotropy of the induced current density (ACID)[51,52] analysis at the PBE/6-311+G(d) level and displayed the results in Figure 6. As shown in Figure 6, the orientation of magnetic field is orthogonal with respect to the ring plane. There is a strong diatropic plotting on two

DOI: 10.1021/acs.jpca.8b10588
J. Phys. Chem. A 2018, 122, 9886−9893

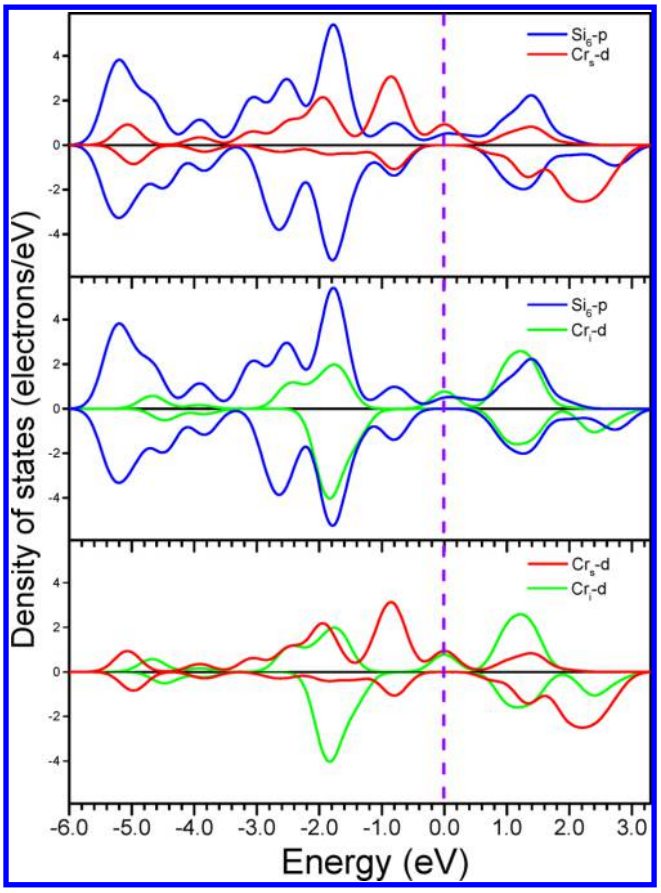

Figure 5. Partial density of states (PDOS) for $Cr_3Si_{12}^-$. Purple dashed line is at the Fermi level.

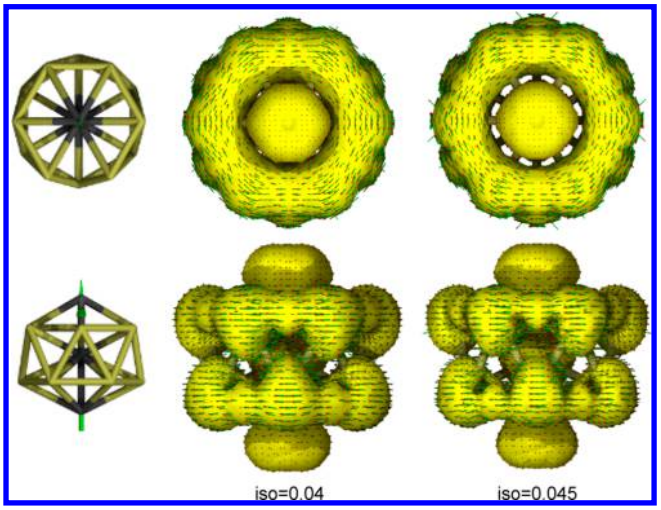

Figure 6. Plots of AICD for $Cr_3Si_{12}^-$ at different isosurface values for top and side views. The external magnetic field vector is orthogonal with respect to the ring plane and points upward.

hexagonal Si_6 rings. The results of ACID analysis demonstrate that the electrons are delocalized strongly on the Si_{12} cages. In addition, the nucleus independent chemical shifts (NICS)[64,65] can also be employed to confirm the electron delocalization of $Cr_3Si_{12}^-$. The NICS(1) value of $Cr_3Si_{12}^-$, which is calculated at the point located 1 Å above the center in direction perpendicular to the ring plane[66] and close to the center of the Si_6 ring, is calculated to be −113 ppm at the GIAO/PBE/6-311+G(d) level. The large negative NICS(1) values of $Cr_3Si_{12}^-$ confirm the results of ACID analysis, indicating that the Si_{12} cage is aromatic.

5. CONCLUSIONS

$Cr_nSi_{15-n}^-$ (n = 1−3) clusters were investigated by using size-selected anion photoelectron spectroscopy. Their structures as well as those of their neutral counterparts were studied with DFT methods. The most stable structure of $CrSi_{14}^-$ is found to be C_{2v} symmetry with the Cr atom encapsulated in a Si_{14} cage. The photoelectron spectrum of $CrSi_{14}^-$ anion confirms that the neutral $CrSi_{14}$ has a large HOMO−LUMO gap. $Cr_2Si_{13}^-$ has two isomers nearly degenerate in energy: one can be characterized as a Si atom interacting with a Cr_2Si_{12} hexagonal prism while the other can be viewed as one Si atom capping a distorted Cr_2Si_{12} hexagonal antiprism. The D_{6d} symmetric wheel structures of $Cr_3Si_{12}^{-/0}$ are much lower in energy than their corresponding second isomers, suggesting that the D_{6d} structures are very stable. The magnetic moments of $CrSi_{14}^-$, $Cr_2Si_{13}^-$, and $Cr_3Si_{12}^-$ increase from 1 to 3 μB and then to 7 μB with the increasing number of Cr atoms in the clusters. The magnetic moments of $Cr_2Si_{13}^-$ and $Cr_3Si_{12}^-$ are mainly contributed by the surface Cr atoms.

■ ASSOCIATED CONTENT

Supporting Information

The Supporting Information is available free of charge on the ACS Publications website at DOI: 10.1021/acs.jpca.8b10588.

NPA charges, atomic moments, and natural electron configuration; the Cartesian coordinates of the low-lying isomers of $Cr_nSi_{15-n}^{-/0}$ (n = 1−3) clusters; simulated photoelectron spectra at the B3LYP/6-311+G(d) level; partial density of states (PDOS) for $Cr_nSi_{15-n}^-$ (n = 1−3) (PDF)

■ AUTHOR INFORMATION

Corresponding Authors

*E-mail: xlxu@iccas.ac.cn.
*E-mail: zhengwj@iccas.ac.cn.

ORCID

Weijun Zheng: 0000-0002-9136-2693

Notes

The authors declare no competing financial interest.

■ ACKNOWLEDGMENTS

This work was supported by the National Natural Science Foundation of China (Grant No. 21273246 and 21103202), the Chinese Academy of Sciences (Grant No. QYZDB-SSW-SLH024), and the Beijing Municipal Science & Technology Commission (Grant No. Z181100004218004). The theoretical calculations were performed on the China Scientific Computing Grid (ScGrid) of the Supercomputing Center, Computer Network Information Center of the Chinese Academy of Sciences.

■ REFERENCES

(1) Hiura, H.; Miyazaki, T.; Kanayama, T. Formation of metal-encapsulating Si cage clusters. *Phys. Rev. Lett.* **2001**, *86*, 1733−1736.
(2) Ohara, M.; Miyajima, K.; Pramann, A.; Nakajima, A.; Kaya, K. Geometric and electronic structures of terbium-silicon mixed clusters ($TbSi_n$; 6 ≤ n ≤ 16). *J. Phys. Chem. A* **2002**, *106*, 3702−3705.

DOI: 10.1021/acs.jpca.8b10588
J. Phys. Chem. A 2018, 122, 9886−9893

(3) Koyasu, K.; Akutsu, M.; Mitsui, M.; Nakajima, A. Selective formation of MSi_{16} (M = Sc, Ti, and V). *J. Am. Chem. Soc.* **2005**, *127*, 4998−4999.
(4) Koyasu, K.; Atobe, J.; Furuse, S.; Nakajima, A. Anion photoelectron spectroscopy of transition metal- and lanthanide metal-silicon clusters: MSi_n^- (n = 6−20). *J. Chem. Phys.* **2008**, *129*, 214301.
(5) Furuse, S.; Koyasu, K.; Atobe, J.; Nakajima, A. Experimental and theoretical characterization of MSi_{16}^-, MGe_{16}^-, MSn_{16}^-, and MPb_{16}^- (M = Ti, Zr, and Hf): The role of cage aromaticity. *J. Chem. Phys.* **2008**, *129*, 064311.
(6) Lyon, J. T.; Gruene, P.; Fielicke, A.; Meijer, G.; Janssens, E.; Claes, P.; Lievens, P. Structures of silicon cluster cations in the gas phase. *J. Am. Chem. Soc.* **2009**, *131*, 1115−1121.
(7) Xu, H. G.; Wu, M. M.; Zhang, Z. G.; Sun, Q.; Zheng, W. J. Structural and bonding properties of $ScSi_n^-$ (n = 2−6) clusters: Photoelectron spectroscopy and density functional calculations. *Chin. Phys. B* **2011**, *20*, 043102.
(8) Xu, H. G.; Wu, M. M.; Zhang, Z. G.; Yuan, J. Y.; Sun, Q.; Zheng, W. J. Photoelectron spectroscopy and density functional calculations of $CuSi_n^-$ (n = 4−18) clusters. *J. Chem. Phys.* **2012**, *136*, 104308.
(9) Xu, H. G.; Zhang, Z. G.; Feng, Y.; Zheng, W. J. Photoelectron spectroscopy and density-functional study of $Sc_2Si_n^-$ (n = 2−6) clusters. *Chem. Phys. Lett.* **2010**, *498*, 22−26.
(10) Gruene, P.; Fielicke, A.; Meijer, G.; Janssens, E.; Ngan, V. T.; Nguyen, M. T.; Lievens, P. Tuning the geometric structure by doping silicon clusters. *ChemPhysChem* **2008**, *9*, 703−706.
(11) Kumar, V.; Kawazoe, Y. Metal-encapsulated fullerenelike and cubic caged clusters of silicon. *Phys. Rev. Lett.* **2001**, *87*, 045503.
(12) Hagelberg, F.; Xiao, C.; Lester, W. A. Cagelike Si_{12} clusters with endohedral Cu, Mo, and W metal atom impurities. *Phys. Rev. B: Condens. Matter Mater. Phys.* **2003**, *67*, 035426.
(13) Sen, P.; Mitas, L. Electronic structure and ground states of transition metals encapsulated in a Si_{12} hexagonal prism cage. *Phys. Rev. B: Condens. Matter Mater. Phys.* **2003**, *68*, 155404.
(14) Lu, J.; Nagase, S. Structural and electronic properties of metal-encapsulated silicon clusters in a large size range. *Phys. Rev. Lett.* **2003**, *90*, 115506.
(15) Mpourmpakis, G.; Froudakis, G. E.; Andriotis, A. N.; Menon, M. Understanding the structure of metal encapsulated Si cages and nanotubes: Role of symmetry and d-band filling. *J. Chem. Phys.* **2003**, *119*, 7498−7502.
(16) Mpourmpakis, G.; Froudakis, G. E.; Andriotis, A. N.; Menon, M. Fe encapsulation by silicon clusters: Ab initio electronic structure calculations. *Phys. Rev. B: Condens. Matter Mater. Phys.* **2003**, *68*, 125407.
(17) Ulises Reveles, J.; Khanna, S. N. Electronic counting rules for the stability of metal-silicon clusters. *Phys. Rev. B: Condens. Matter Mater. Phys.* **2006**, *74*, 035435.
(18) Zdetsis, A. D. Bonding and structural characteristics of Zn-, Cu-, and Ni-encapsulated Si clusters: Density-functional theory calculations. *Phys. Rev. B: Condens. Matter Mater. Phys.* **2007**, *75*, 085409.
(19) Jhabvala, M.; Babu, R. S.; Monroy, C.; Freund, M. M.; Dowell, C. D. Development of low-noise high value chromium silicide resistors for cryogenic detector applications. *Cryogenics* **2002**, *42*, 517−526.
(20) Beck, S. M. Studies of silicon cluster metal atom compound formation in a supersonic molecular beam. *J. Chem. Phys.* **1987**, *87*, 4233−4234.
(21) Beck, S. M. Mixed metal-silicon clusters formed by chemical-reaction in a supersonic molecular beam: Implications for reactions at the metal/silicon interface. *J. Chem. Phys.* **1989**, *90*, 6306−6312.
(22) Zheng, W. J.; Nilles, J. M.; Radisic, D.; Bowen, K. H. Photoelectron spectroscopy of chromium-doped silicon cluster anions. *J. Chem. Phys.* **2005**, *122*, 071101.
(23) Kong, X. Y.; Xu, H. G.; Zheng, W. J. Structures and magnetic properties of $CrSi_n^-$ (n = 3−12) clusters: photoelectron spectroscopy and density functional calculations. *J. Chem. Phys.* **2012**, *137*, 064307.
(24) Neukermans, S.; Wang, X.; Veldeman, N.; Janssens, E.; Silverans, R. E.; Lievens, P. Mass spectrometric stability study of binary MS_n clusters (S = Si, Ge, Sn, Pb, and M = Cr, Mn, Cu, Zn). *Int. J. Mass Spectrom.* **2006**, *252*, 145−150.
(25) Han, J. G.; Hagelberg, F. A density functional theory investigation of $CrSi_n$ (n = 1−6) clusters. *Chem. Phys.* **2001**, *263*, 255−262.
(26) Han, J. G.; Shi, Y. Y. A computational study on geometries, electronic structures and ionization potentials of MSi_{15} (M = Cr, Mo, W) clusters by density functional method. *Chem. Phys.* **2001**, *266*, 33−40.
(27) Kawamura, H.; Kumar, V.; Kawazoe, Y. Growth, magic behavior, and electronic and vibrational properties of Cr-doped Si clusters. *Phys. Rev. B: Condens. Matter Mater. Phys.* **2004**, *70*, 245433.
(28) Guo, L. J.; Zhao, G. F.; Gu, Y. Z.; Liu, X.; Zeng, Z. Density-functional investigation of metal-silicon cage clusters MSi_n (M = Sc, Ti, V, Cr, Mn, Fe, Co, Ni, Cu, Zn; n = 8−16). *Phys. Rev. B: Condens. Matter Mater. Phys.* **2008**, *77*, 195417.
(29) Abreu, M. B.; Reber, A. C.; Khanna, S. N. Does the 18-electron rule apply to $CrSi_{12}$? *J. Phys. Chem. Lett.* **2014**, *5*, 3492−3496.
(30) Khanna, S. N.; Rao, B. K.; Jena, P. Magic numbers in metallo-inorganic clusters: Chromium encapsulated in silicon cages. *Phys. Rev. Lett.* **2002**, *89*, 016803.
(31) He, J. G.; Wu, K. C.; Liu, C. P.; Sa, R. J. Stabilities of 3d transition-metal doped Si_{14} clusters. *Chem. Phys. Lett.* **2009**, *483*, 30−34.
(32) Kumar, V.; Kawazoe, Y. Magic behavior of $Si_{15}M$ and $Si_{16}M$ (M = Cr, Mo, and W) clusters. *Phys. Rev. B: Condens. Matter Mater. Phys.* **2002**, *65*, 073404.
(33) Wang, J.; Ma, Q. M.; Xu, R. P.; Liu, Y.; Li, Y. C. 3d transition metals: Which is the ideal guest for Si_n (n = 15, 16) cages? *Phys. Lett. A* **2009**, *373*, 2869−2875.
(34) Robles, R.; Khanna, S. N.; Castleman, A. W. Stability and magnetic properties of T_2Si_n (T = Cr, Mn, $1 \leq n \leq 8$) clusters. *Phys. Rev. B: Condens. Matter Mater. Phys.* **2008**, *77*, 235441.
(35) Ji, W. X.; Luo, C. L. Structures, magnetic properties, and electronic counting rule of metals-encapsulated cage-like M_2Si_{18} (M = Ti-Zn) clusters. *Int. J. Quantum Chem.* **2012**, *112*, 2525−2531.
(36) Xu, H. G.; Zhang, Z. G.; Feng, Y.; Yuan, J. Y.; Zhao, Y. C.; Zheng, W. J. Vanadium-doped small silicon clusters: Photoelectron spectroscopy and density-functional calculations. *Chem. Phys. Lett.* **2010**, *487*, 204−208.
(37) Lv, J.; Wang, Y.; Zhu, L.; Ma, Y. Particle-swarm structure prediction on clusters. *J. Chem. Phys.* **2012**, *137*, 084104.
(38) Wang, Y. C.; Lv, J.; Zhu, L.; Ma, Y. M. CALYPSO: A method for crystal structure prediction. *Comput. Phys. Commun.* **2012**, *183*, 2063−2070.
(39) Frisch, M. J.; Trucks, G. W.; Schlegel, H. B.; Scuseria, G. E.; Robb, M. A.; Cheeseman, J. R.; Scalmani, G.; Barone, V.; Mennucci, B.; Petersson, G. A. et al. *GAUSSIAN 09*, Revision A.02; Gaussian, Inc.: Wallingford, CT, 2009.
(40) Perdew, J. P.; Burke, K.; Ernzerhof, M. Generalized gradient approximation made simple. *Phys. Rev. Lett.* **1996**, *77*, 3865−3868.
(41) Dobbs, K. D.; Hehre, W. J. Molecular orbital theory of the properties of inorganic and organometallic compounds 5. Extended basis sets for first-row transition metals. *J. Comput. Chem.* **1987**, *8*, 861−879.
(42) Gordon, M. S.; Binkley, J. S.; Pople, J. A.; Pietro, W. J.; Hehre, W. J. Self-consistent molecular-orbital methods. 22. Small split-valence basis sets for second-row elements. *J. Am. Chem. Soc.* **1982**, *104*, 2797−2803.
(43) Foster, J. P.; Weinhold, F. Natural hybrid orbitals. *J. Am. Chem. Soc.* **1980**, *102*, 7211−7218.
(44) Reed, A. E.; Weinhold, F. Natural bond orbital analysis of near-Hartree-Fock water dimer. *J. Chem. Phys.* **1983**, *78*, 4066−4073.
(45) Reed, A. E.; Weinstock, R. B.; Weinhold, F. Natural population analysis. *J. Chem. Phys.* **1985**, *83*, 735−746.
(46) Reed, A. E.; Weinhold, F. Natural localized molecular-orbitals. *J. Chem. Phys.* **1985**, *83*, 1736−1740.

DOI: 10.1021/acs.jpca.8b10588
J. Phys. Chem. A 2018, 122, 9886−9893

(47) Carpenter, J. E. *Extension of lewis structure concepts to open-shell and excited-state molecular species*; Ph.D. thesis, University of Wisconsin-Madison, 1987.
(48) Carpenter, J. E.; Weinhold, F. Analysis of the geometry of the hydroxymethyl radical by the "different hybrids for different spins" natural bond orbital procedure. *J. Mol. Struct.: THEOCHEM* **1988**, *169*, 41−62.
(49) Weinhold, F.; Carpenter, J. E. *The structure of small molecules and ions*; Plenum: New York, 1988.
(50) Reed, A. E.; Curtiss, L. A.; Weinhold, F. Intermolecular interactions from a natural bond orbital, donor-acceptor viewpoint. *Chem. Rev.* **1988**, *88*, 899−926.
(51) Herges, R.; Geuenich, D. Delocalization of electrons in molecules. *J. Phys. Chem. A* **2001**, *105*, 3214−3220.
(52) Geuenich, D.; Hess, K.; Kohler, F.; Herges, R. Anisotropy of the induced current density (ACID), a general method to quantify and visualize electronic delocalization. *Chem. Rev.* **2005**, *105*, 3758−3772.
(53) Lu, T.; Chen, F. Multiwfn: a multifunctional wavefunction analyzer. *J. Comput. Chem.* **2012**, *33*, 580−92.
(54) Lee, C. T.; Yang, W. T.; Parr, R. G. Development of the colle-salvetti correlation-energy formula into a functional of the electron-density. *Phys. Rev. B: Condens. Matter Mater. Phys.* **1988**, *37*, 785−789.
(55) Becke, A. D. Density-functional thermochemistry. 3. The role of exact exchange. *J. Chem. Phys.* **1993**, *98*, 5648−5652.
(56) Tozer, D. J.; Handy, N. C. Improving virtual Kohn-Sham orbitals and eigenvalues: Application to excitation energies and static polarizabilities. *J. Chem. Phys.* **1998**, *109*, 10180−10189.
(57) Akola, J.; Manninen, M.; Häkkinen, H.; Landman, U.; Li, X.; Wang, L. S. Photoelectron spectra of aluminum cluster anions: Temperature effects andab initiosimulations. *Phys. Rev. B: Condens. Matter Mater. Phys.* **1999**, *60*, R11297−R11300.
(58) Rata, I.; Shvartsburg, A. A.; Horoi, M.; Frauenheim, T.; Siu, K. W.; Jackson, K. A. Single-parent evolution algorithm and the optimization of Si clusters. *Phys. Rev. Lett.* **2000**, *85*, 546−9.
(59) Wu, X.; Liang, X. Q.; Du, Q. Y.; Zhao, J. J.; Chen, M.; Lin, M. D.; Wang, J. S.; Yin, G. J.; Ma, L.; King, R. B.; et al. Medium-sized Si_n^- (n = 14−20) clusters: a combined study of photoelectron spectroscopy and DFT calculations. *J. Phys.: Condens. Matter* **2018**, *30*, 354002.
(60) Huang, X. M.; Xu, H. G.; Lu, S. J.; Su, Y.; King, R. B.; Zhao, J.; Zheng, W. J. Discovery of a silicon-based ferrimagnetic wheel structure in $V_xSi_{12}^-$ (x = 1−3) clusters: photoelectron spectroscopy and density functional theory investigation. *Nanoscale* **2014**, *6*, 14617−21.
(61) Huang, X. M.; Lu, S. J.; Liang, X. Q.; Su, Y.; Sai, L. W.; Zhang, Z. G.; Zhao, J. J.; Xu, H. G.; Zheng, W. J. Structures and electronic properties of $V_3Si_n^-$ (n = 3−14) clusters: A combined ab initio and experimental study. *J. Phys. Chem. C* **2015**, *119*, 10987−10994.
(62) Michalopoulos, D. L.; Geusic, M. E.; Hansen, S. G.; Powers, D. E.; Smalley, R. E. The bond length of Cr_2. *J. Phys. Chem.* **1982**, *86*, 3914−3916.
(63) Hull, A. W. X-ray crystal analysis of thirteen common metals. *Phys. Rev.* **1921**, *17*, 571−588.
(64) Schleyer, P. V. R.; Maerker, C.; Dransfeld, A.; Jiao, H.; van Eikema Hommes, N. J. R. Nucleus-independent chemical shifts: A simple and efficient aromaticity probe. *J. Am. Chem. Soc.* **1996**, *118*, 6317−6318.
(65) Chen, Z.; Wannere, C. S.; Corminboeuf, C.; Puchta, R.; Schleyer, P. Nucleus-independent chemical shifts (NICS) as an aromaticity criterion. *Chem. Rev.* **2005**, *105*, 3842−3888.
(66) Zborowski, K. K.; Sola, M.; Poater, J.; Proniewicz, L. M. Aromatic properties of 8-hydroxyquinoline and its metal complexes. *Cent. Eur. J. Chem.* **2013**, *11*, 655−663.

DOI: 10.1021/acs.jpca.8b10588
J. Phys. Chem. A 2018, 122, 9886−9893